Grain size dependence of the strength of metals: The Hall-Petch effect does not scale as the inverse square root of grain size

D.J. Dunstan[a]* and A.J. Bushby[b]
[a] School of Physics and Astronomy, [b] School of Engineering and Materials Science,
Queen Mary University of London,
London E1 4NS, UK.

* Corresponding author: Tel 44 207 882 3411, Fax 44 207 882 7033,
**Emails: d.dunstan@qmul.ac.uk and a.j.bushby@qmul.ac.uk**

Highlights

- Little experimental evidence supports the Hall-Petch inverse square-root scaling exponent.
- The data fits a simple inverse scaling law.
- The Hall-Petch effect is the same size effect as observed in micro-mechanics.

Abstract: The classic data in the literature for the grain size dependence of the strength in many metals are reviewed. The exponent x relating strength to grain size d^{-x} is not often the eponymous inverse square-root relationship (known as the Hall-Petch effect), but is widely scattered from values as low as $x = 0.2$ to values as high as $x = 1$. These exponents for individual datasets are shown to be largely meaningless. For an ensemble of n selected datasets, the fit to the functional form $\ln[d]/d + const$ with $n + 1$ free fitting parameters is found to be almost as good as the fit to $1/Sqrt[d] + const$ with $2n$ fitting parameters (the Hall-Petch fit). The probability that the former is the preferable fit is high. Some data sets do not agree with the $\ln[d]/d$ fit, but their deviation is readily explained on simple physical grounds. Moreover, even when they are included in the fit, statistical tests still show that the $\ln[d]/d$ form is preferable by a wide margin. The conclusion is that the Hall-Petch effect is not another size effect *sui generis* but is the same size effect as that observed in epitaxial thin film growth and in micromechanical testing of small specimens. Consequently we propose that grain size strengthening of metals is driven by constraints on stress and dislocation curvature according to the space available.

Graphical Abstract:
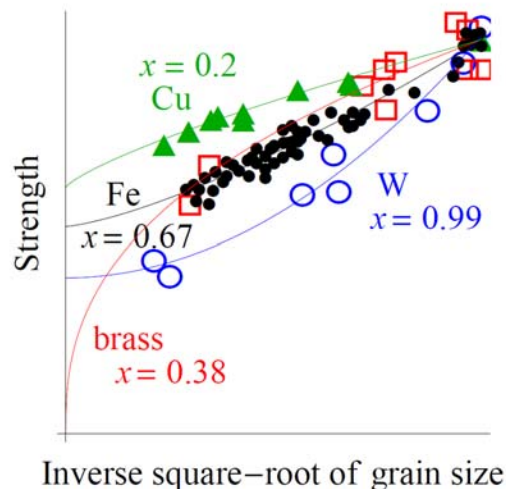
1. Introduction

The apparent increase in strength of a material as the size of the specimen or the strain field or some dimension of the material microstructure is reduced is known as size-dependent plasticity. This size effect is now well-established in many forms of micromechanical testing. It is manifested in an increase of the apparent strength of a material in the form of thin foils in flexure (e.g. Ehrler *et al.*, 2008), thin wires in torsion (e.g. Dunstan *et al.*, 2009; Liu *et al.*, 2013) and perhaps in tension (e.g. Bushby and Dunstan, 2011), micropillars in compression (see Korte and Clegg, 2010, for a compilation of much data), in foams (e.g. Hodge *et al.*, 2007)) and in other geometries such as indentation hardness testing (e.g. Bushby & Dunstan, 2004). For reviews, see Arzt (1998), Zhu *et al.* (2008) or Kraft *et al.* (2010). The size effect is reported often in the yield point, to whatever accuracy that may be established in different experiments, and often in the flow stress at higher plastic strain. Many authors have described it in terms of a power-law dependence of yield or flow stress σ on the relevant size,

$$\sigma = \sigma_0 + k\ell^{-x} \tag{1}$$

where ℓ is the relevant size, and then sought to interpret the scaling exponent x phenomenologically or in terms of the underlying physics. The constants σ_0 and k are expected to be material constants; e.g. σ_0 may be the Peierls stress, or it may be the strength due to work-hardening. We refer to the other term in Eq.1, $(\sigma - \sigma_0)$, as the overstress that is to be explained here by the grain-size dependence.

Hall (1951) and Petch (1953) presented data and fits showing that the strength of iron and steel depends on the grain size d, following Eq.1 (ℓ identified with d) with an exponent of $x = \frac{1}{2}$ and a coefficient k_{HP} which is considered to be a material parameter. There is a large body of data in the literature reinforcing this dependence in a very wide range of metals, and so the equation

$$\sigma = \sigma_0 + \frac{k_{HP}}{\sqrt{d}} \tag{2}$$

is presented in the textbooks as the Hall-Petch effect. Theories of the effect will be considered in Section 3.1 below.

Recently, we presented an analysis of micromechanical testing data (Dunstan and Bushby, 2013), particularly compression testing of micropillars, in which we showed that the data for the yield or flow stress of the pillars as a function of pillar diameter, while consistent with scaling exponents in the range 0 to 1, are also consistent with a fixed exponent $x = 1$ and with a fixed prefactor k,

$$\sigma = \sigma_0 + k\ell^{-1} \tag{3}$$

and also with the very similar equation,

$$\sigma = \sigma_0 + k \ln \ell \, \ell^{-1} \tag{4}$$

There are physical reasons why these equations might be good descriptions of the data, especially Eq.4; this is discussed in Section 3.2 below. The purpose of this paper, therefore, is to review some of the classic literature data which demonstrates the Hall-Petch effect, to assess whether the Hall-Petch scaling exponent in the data is accurately $x = \frac{1}{2}$ or whether the data is better described by Eq.3 or Eq.4, and thereby to determine whether the Hall-Petch effect is *sui generis* or whether it is another manifestation of the same size effect that is seen in micromechanical testing.

2. Experimental data

2.1. *Determination of the Scaling Exponent*

In Fig.1 we present some of the classic data upon which was based the Hall-Petch formula, Eq.2, in which σ may be the yield or flow stress measured directly or may be derived from a hardness measurement. It is not necessary in this paper to distinguish yield and flow stress: experimentally, a reported yield stress may merely represent the flow stress at the lowest resolvable strain, and in any case the grain-size effect is reported in both yield and flow stress.

The data are rescaled by the minimum grain size and the maximum stress of each dataset in order to display them on the same axes. The tungsten dataset used here is given by Vashi *et al*. (1970) and obtained by indentation. We have divided the diamond pyramid hardness (DPH) values presented by the factor 2.7 to estimate the flow stresses. The data for iron are those of Petch (1953) which are for mild steel and two kinds of iron, but the data for the three materials are so similar that there is no need to distinguish them. The data for copper and brass are taken from Armstrong *et al.* (1962). In Fig.1a, the four datasets are plotted against the inverse square-root of d, as was done by the original authors, rescaled so that they can be represented on the same graph. The solid lines in Fig.1a are least-squares linear regression fits to Eq.2, and they fit the data well. These datasets and fits are typical of the large body of experimental evidence for Eq.2 for the Hall-Petch effect.

In Fig.1b, the same data are plotted against the inverse fourth-root of d, and in Fig.1c they are plotted against the inverse of d. The solid lines are least-squares fits of the data to Eq.1 with $x = \frac{1}{4}$ and with $x = 1$, and they are clearly good fits to the data – often as good, to the eye, as the fits to $x = \frac{1}{2}$ of Fig.1a. In Fig.1d are plotted least-squares fits to Eq.1 in which x is a free fitting parameter as well; in this plot the same axes are used as in Fig.1a. Values of x ranging from 0.2 to 1 are found for the different datasets (Table I). Thus the good fits to the inverse square-root of d in Fig.1a are not, of themselves, strong evidence for the scaling exponent being $x = \frac{1}{2}$.
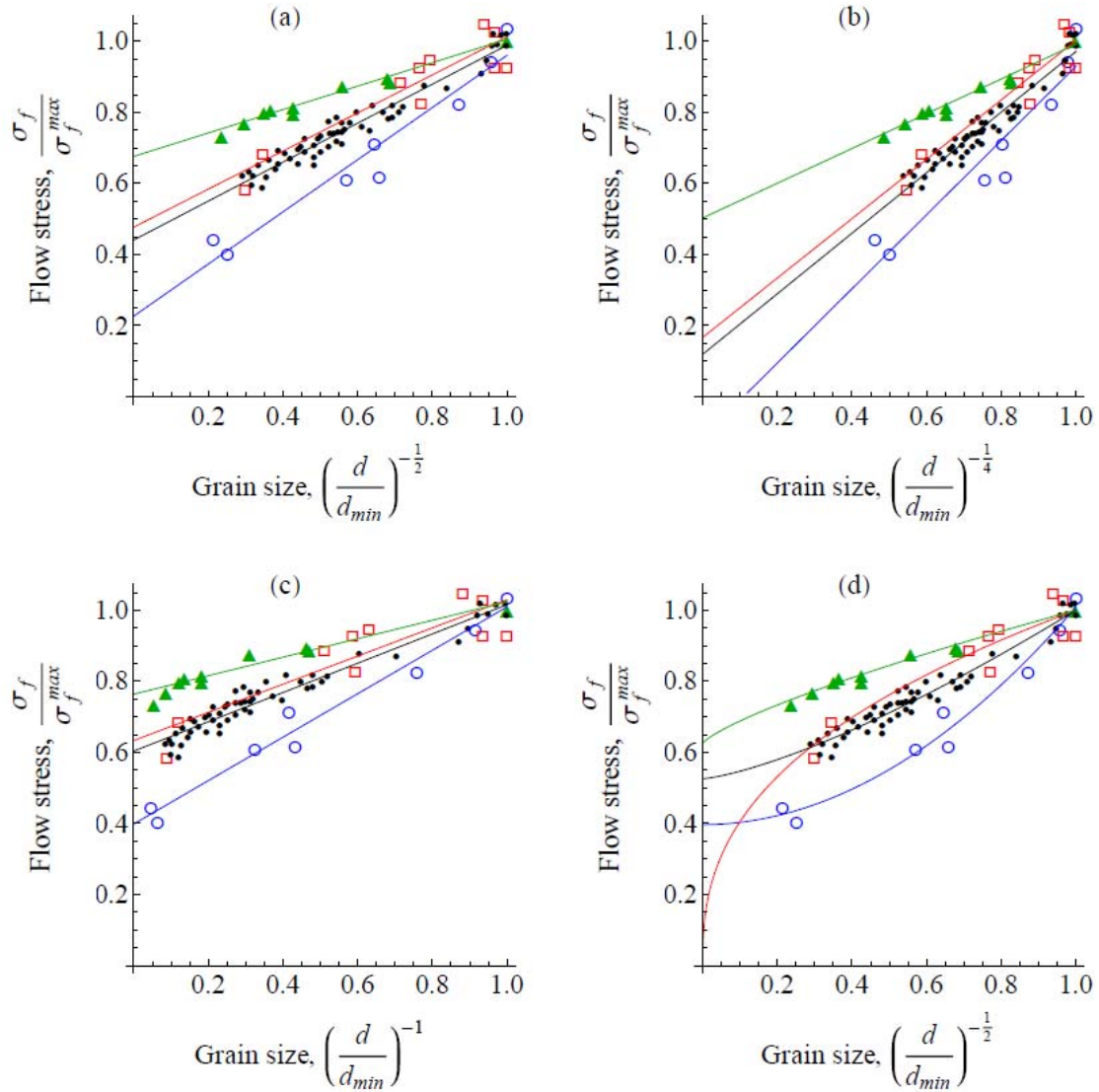
4

Fig.1. Scaled data demonstrating the Hall-Petch effect for W (open circles) from Vashi *et al.* (1970), for Fe (small points) from Petch (1953), and for Cu (solid triangles) and brass (open squares) from Armstrong *et al.* (1962). Each dataset is scaled by its minimum grain size and maximum flow stress in order that the datasets may be compared on the same axes. In (a), the data are plotted against the inverse square-root of the grain size and the solid lines are best fits of the Hall-Petch formula Eq.2 to the data. In (b) and (c), the data are plotted against the inverse fourth-root and the inverse of the grain size, and the solid lines are fits of the general expression Eq.1 with $x = ¼$ and $x = 1$ respectively. In (d) the data are plotted as in (a) but compared with the non-linear fits of Eq.1 to the data in which σ_0, k and x have all been taken as free fitting parameters. The fitted values of the exponent x are 0.99 for W, 0.67 for Fe, 0.38 for brass and 0.2 for Cu.

We have shown previously that scaling exponents cannot be reliably obtained from plots and fits such as those in Fig.1a-c. Given their scatter, the data do not cover a sufficient range of grain sizes. Considerably more than two decades in grain size would be required before any confidence could be placed in the value of the exponent revealed by straight-line fits such as those in Fig.1a (Dunstan and Bushby, 2013). The fitted exponents of Fig.1d are also not reliable – indeed, we would suggest, not meaningful – for inspection of Fig.1d shows that the curvatures corresponding to values of $x \neq \frac{1}{2}$ are largely determined by the data points for the very largest grain sizes. Yet the four datasets used in Fig.1 are typical of the datasets in the literature. We chose these four for Fig.1 because they display the full range of fitted exponents x, from 0.2 to 1. In Table I we give fitting parameters for many more datasets for a variety of different metals from the literature, which again display a wide range of fitted values for the scaling exponent x. The standard deviations on the fitted exponents x are also given, and it is clear from them that the data does not give a precise determination of the exponents.

It is essential, in displaying agreement between data and a particular analytic fit as in Fig.1a, to consider also what else the data fits or does not fit, before concluding that the data supports the chosen analytic fit. We conclude that this collection of classic data, whether as individual datasets or taken as a whole, gives no significant experimental support to the inverse square-root dependence of the Hall-Petch effect on grain size, Eq.2.

2.2. *Other Fits*

We noted in the Introduction that there are good physical reasons to expect that the data might fit Eq.3 or Eq.4. Of these, Eq.4 is the more theoretically precise. These equations derive most fundamentally from the relationship between dislocation curvature and stress (Orowan, 1947), through the elastic energy that can be relieved by the creation or evolution of dislocations and the energy required for the creation or evolution of the dislocations (Dunstan *et al.*, 1996). Both of these energies depend similarly on the elastic moduli of the material, and the only length scale in the problem is the Burgers vector of the dislocations. The Young's modulus may be taken as representative of the different moduli that enter into the stored elastic energy in different experiments and into the dislocation self-energy. Without entering into the details of what dislocations are available in each metal, the Burgers vector scales with the lattice parameter of the material. Before making any comparison with Eq.3 or Eq.4, therefore, it is appropriate to apply the two normalisations, dividing the stress by the Young's modulus Y and dividing the grain size by the lattice parameter, a_0. Then we plot the normalised stress, which is the elastic strain $\varepsilon = \sigma/Y$, against the normalised grain size d/a_0. Fitting the normalised data to Eqs. 1–4 gives the dimensionless fitting parameters ε_0, k and x reported in Table I.

Seventeen datasets from the literature (references in Table I) for various metals were normalised in this way and compared with Eq.4. Eight which agreed reasonably well are plotted on logarithmic axes in Fig.2a and 2b. The solid lines in Fig.2a are not fits to the data but plots of Eq.4 with a single value of k and values of σ_0 chosen to display the consistency of the data with Eq.4. In Fig.2b, the same data are plotted together with fits of the Hall-Petch relation, Eq.2 (the normalised fitting parameters are given in Table 1). The remaining nine datasets are plotted in Fig.2c for comparison with Eq.4 and again in Fig.2d with their Hall-Petch fits.
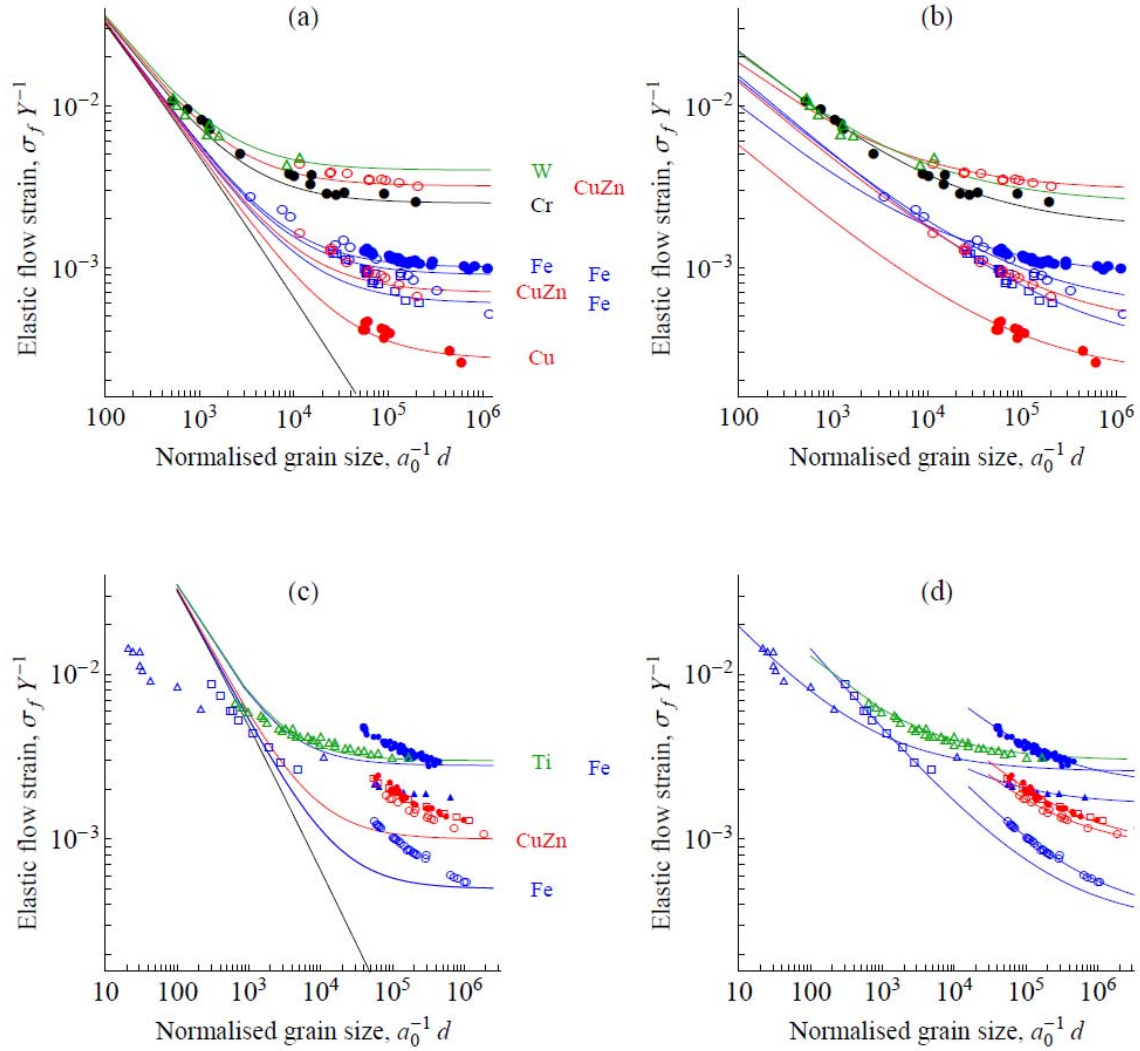
Fig.2. Data for flow stress or hardness are normalised as described in the text. In (a) and (b), those datasets which agree reasonably well with Eq.3 are plotted. In (c) and (d), the datasets which are in significant disagreement with Eq.3 are shown. The solid lines in (a) and (c) represent Eq.4 with $x = 1$ and $k = 1$; only σ_0 is varied to fit each dataset. The solid lines in (b) and (d) are fits to Eq.2 with $x = \frac{1}{2}$; both k and σ_0 are varied to fit each dataset. The sources for the data and values of the fitting parameters are given in Table I.

The behaviour revealed by Fig.2 is very interesting. It is certainly the case that if the yield or flow stress were actually determined by the Hall-Petch formula, Eq.2, with the scaling exponent fixed at $x = \frac{1}{2}$ and the two fitting parameters ε_0 and k_{HP} independent and determined by different physical mechanisms, it would be implausible that ε_0 and k should be related in a large proportion of the data sets in such a way as to permit the fits

7

of Fig.2a to the one-free-parameter formula, Eq.4, with $x = 1$, $k \sim 1$ and only ε_0 free. Then it is plausible that those datasets which do not agree (Fig.2c, d) show that there are other physical processes which often modify the behaviour from that expected from Eq.4. This is discussed in the next Section.

2.3. *Other Physical Processes*

The nine datasets of Fig.2c deviate sufficiently from Eq.4 that we need to consider whether they refute it, or whether their deviation can be accounted for by plausible physical mechanisms. Consider first the data for nanocrystalline iron (Armstrong, 2011) and Ti (Hu and Cline, 1968). At small grain sizes (normalised d of 1000 or less), these three datasets deviate considerably below the Eq.4 line, so that if a fit to Eq.4 is forced, much lower values of k are required (Table 1). However, nanocrystalline metals are expected to fall below the strength predicted by the Hall-Petch law in any case, for example because the mechanism of plasticity may become grain-boundary sliding. See Arzt (1998) and Armstrong (2011) for detailed discussions. So these three datasets do not refute Eq.4.

The other six datasets in Fig.2c are in disagreement with Eq.4 at large grain sizes. The strength decrease with increasing grain size is much greater than predicted. This is explicable if for example we suppose that the metallurgical processing that creates the large grain material also softens it – e.g. by reducing dislocation densities. This softening will then be correlated with the grain size but not caused by it. If a fit to Eq.4 is forced, much higher values of k are required (Table 1). Other mechanisms, such as a correlation between grain size and precipitate densities, might also be invoked. However, the papers from which we obtained these datasets mostly do not give sufficient details of the preparation and characterisation to enable an assessment of the magnitude of these effects. Moreover, grain size distributions and the methods of finding the average are not generally given. There is considerable scope for inconsistency between different authors.

To summarise the implications of the experimental data, Fig.2b and 2d show that Eq.2 fits all the data well, with widely scattered parameters ε_0 and k_{HP} which can take on arbitrary values (i.e. there is no reliable theoretical prediction of these values for different materials, see Section 3.1). But there is little evidence that the exponent is $x = \frac{1}{2}$ for all materials. On the other hand, Fig.2a reveals an unexpected behaviour that requires explanation. It shows that, with an exponent $x = 1$ (Eq.3) or close to that (Eq.4), many values of k for many materials collapse onto a single value, $k \sim 1$. This suggest the hypothesis that Eq.4 correctly describes the general behaviour, with special circumstances (grain boundary slipping, changes of strength induced by the metallurgical processing and correlated with but not causally related to grain size, etc.) causing large deviations from Eq.4 in about half the datasets. In the next section we test this hypothesis more rigorously.

2.4. *Statistical Analysis*

Here we follow the analysis methodology of McKay (2003) to calculate the likelihoods of the hypotheses given all the available data (without the discrimination of Fig.2). Then we use the Akaike information criterion (AIC, Akaike, 1974) to determine

and quantify a preference for one hypothesis over the other. The AIC is a well-established criterion that takes into account the number of parameters as well as the data itself. There are developments of it, e.g. the corrected Akaike information criterion (AICc) and the Bayesian information criterion (BIC), which generally penalise the number of parameters more severely than the AIC (Liddle, 2007), so that the use of the AIC here is conservative.

We restrict our analysis to the two hypotheses or models, $\mathbf{H}_{HP}$ and $\mathbf{H}_{DC}$ (the subscript DC indicating the role played by dislocation curvature) expressed by Eq.2 and Eq.4 respectively. That is, $\mathbf{H}_{HP}$ is the hypothesis that Eq.2 describes the physics and the data correctly, with $x = \frac{1}{2}$ and with σ_0 and k_{HP} as fitting parameters which depend on the material and on the specimen preparation. $\mathbf{H}_{DC}$ is the hypothesis that Eq.4 describes the physics and the data correctly, with $x = 1$, with $k \sim 1$ and with only σ_0 as a fitting parameter which depends on the material and on the specimen preparation. We test these hypotheses against the full seventeen datasets.

Independent fits to Eq.4 were made so that each data set is described by a pair of values $d_i = (\sigma_0, k)$. We write the full set of pairs as $\mathbf{d} = \{\sigma_0, k\}$. These are given in Table 1 as well as the Hall-Petch σ_0 and k. For all fits reported here, we used the *Mathematica*$^{©}$ function *NonlinearModelFit*, which returns many statistical diagnostics. However, it is clear that the contributions to residuals discussed in Section 2.3 will not give Gaussian-distributed independent residuals, but instead very heavy-tailed distributions of correlated residuals. Consequently, many of the diagnostics must be treated with caution.
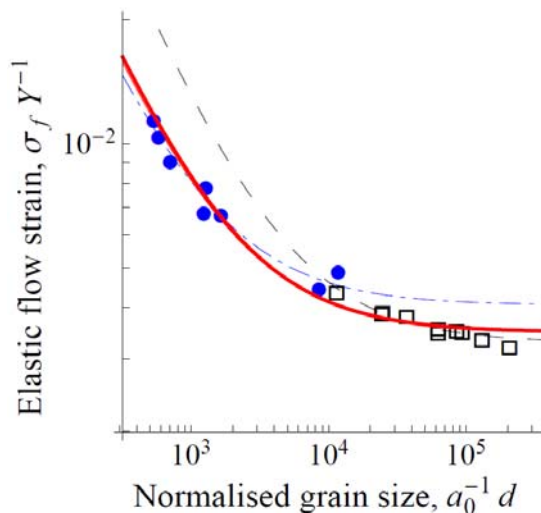

Fig. 3. The dataset for tungsten (solid circles) and a dataset for brass (CuZn20, open squares) are plotted on log-log axes. The two-parameter fits of Eq.4 are (W) the chain-dotted line and (CuZn20) the dashed line. The one-parameter fits with $k = 0.7$ are shown by the solid lines which are (by chance) indistinguishable for these two datasets.

The fitted values are highly correlated; the off-diagonal elements of the correlation matrix are close to unity. We therefore also fixed k (at 0.7) and, fitting only for different values of σ_0 for each dataset, obtained satisfactory fits for the datasets in Fig.2a while for the other nine materials these one-parameter fits with fixed k are plainly bad as in Fig.2c. In Fig.3 the two-parameter fits for W and for CuZn20 are shown as

broken lines and the one-parameter fits (by chance, indistinguishable from each other) as the heavy solid line. Here and for the other materials in Table I from W through to CuZn20 the one-parameter fits are acceptable, so we carried out a nine-parameter fit to all eight of these data sets with the eight values of σ_0 and a single value of k as the free parameters. This fit returned $k = 0.68$. The root-mean-square average of the residuals was 2.3×10^{-4}. For comparison, a 16-parameter fit (eight values of σ_0 and eight value of k_{HP} with $x = \frac{1}{2}$) to Eq.2 gives an RMS average residual of 1.8×10^{-4}. This difference is reflected in the adjusted R^2 values of 0.995 and 0.997 respectively. Both fits are good, but the 16-parameter fit is better than the 9-parameter fit, with smaller residuals and a larger R^2. This is expected, even if both models were good descriptions of the data. The $\mathbf{H}_{HP}$ fit with more parameters should have smaller residuals simply because it has more parameters (it is expected from Fig.1 that the lower value of the exponent x in $\mathbf{H}_{HP}$, even if incorrect, makes little difference to the quality of fit). Indeed, if we fitted all three parameters of Eqn.1, the residuals would be reduced below those of $\mathbf{H}_{HP}$, but there would be 24 free fitting parameters. The key point is that the quality of the fit is not here the determining factor in deciding which hypothesis is favoured by the data.

In order to know which of the two hypotheses is selected by the data, we apply the Akaike information criterion (AIC). Following McKay (2003), we first estimate the likelihood of the two hypotheses in the light of the data. The likelihood function of a hypothesis $\mathbf{H}$ given a datum x is the probability of the datum x under the hypothesis,

$$L(\mathbf{H}|x) = P(x|\mathbf{H}) \qquad (5)$$

and for a dataset $\mathbf{x}$, also written as $\{x_i\}$ of n data x_i, the likelihood is the product of the likelihoods of Eq.5 for each datum,

$$L(\mathbf{H}|\mathbf{x}) = \prod_{i=1}^{n} P(x_i|\mathbf{H}) \qquad (6)$$

The absolute value of the likelihood is of no significance; hypothesis preferences are concerned only with the relative values for the different hypotheses (McKay, 2003).
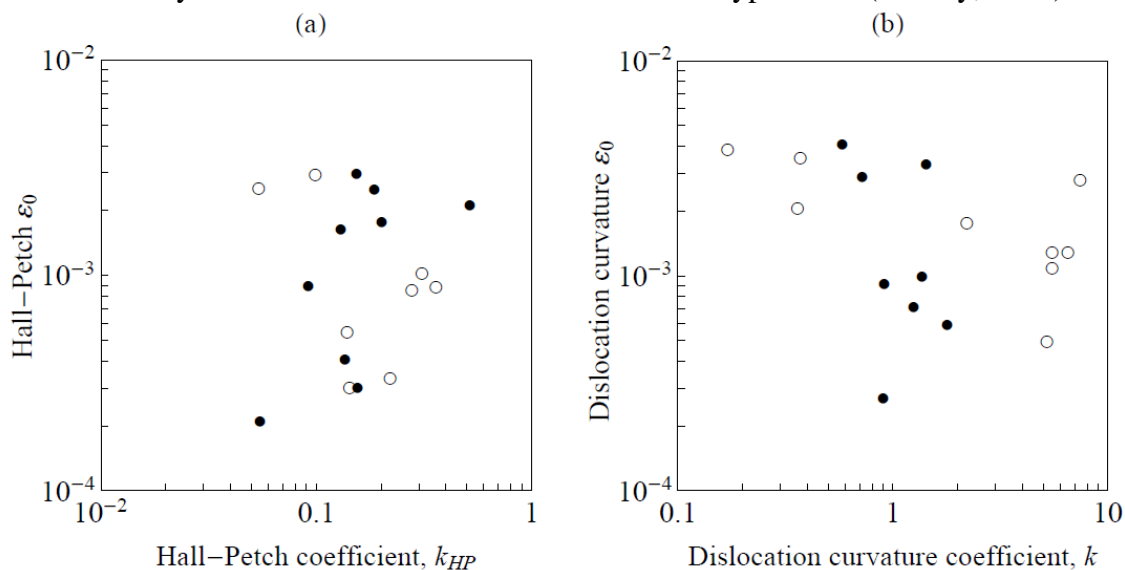

Fig.4. Plots of the fitted coefficients normalised by the Young's modulus and the lattice constant (Table I), (a) ε_0 and k_{HP} for the Hall-Petch fits to Eqn.2,

10

and (b) ε_0 and k for the fits to Eq.4. The datasets shown in Fig.2a are plotted as solid circles. In (a), there are no expectations where these should be in the ε_0-k_{HP} space, while in (b) they are expected to lie close to $k \sim 1$. The open circles represent the datasets plotted in Fig.2c; there are no expectations where these should be in (a).

Rather than considering each individual datum, we analyse the set **d** of pairs of parameters $d_i = (\varepsilon_0, k)$ for each of the seventeen datasets of Fig.2. Under $\mathbf{H}_{HP}$, any such pair is consistent with the hypothesis. In Fig.3a, the experimental values are scattered within a domain of approximately 1 decade wide by 1.5 decades high. By Benford's Law, without any theory to suggest what values should be observed, data are expected to be uniformly distributed on a logarithmic scale (Newcomb, 1881; Benford, 1938) This is indeed observed in Fig.3a, for both the data of Fig.2a (solid points) and the data of Fig.2c (open circles). The Eq.4 fitted values $\mathbf{d} = \{(\sigma_0, k)\}$ are plotted in Fig.3b. The solid data points are now grouped in the middle of the plot. This might be considered to be an artefact of the initial selection of some datasets for Fig.2a and others for Fig.2c. However, we now proceed without making any use of this selection.

In the space of Fig.2b, the Hall-Petch Eq.2, model $\mathbf{H}_{HP}$ predicts a flat distribution of $P(x_i|\mathbf{H}_{HP})$. We are not interested in the distribution over ε_0, which is the same for both hypotheses. We may choose suitable units for the probability density distribution over k. We choose probability per two decades of k, over the range $k_L = \log_{10} k$ from $k_L = -1$ to 1. Then $P(x_i|\mathbf{H}_{HP}) = 1$ throughout this range and $L(\mathbf{x}|\mathbf{H}_{HP}) = P(\mathbf{x}|\mathbf{H}_{HP}) = 1^{17} = 1$. Eq.4, model $\mathbf{H}_{DC}$, predicts a heavy-tailed probability density distribution centred on some value of k_L and with an unknown width Δk_L. That is, the hypothesis contains two variables and may be written as $\mathbf{H}_{DC}(k_L, \Delta k_L)$. The likelihood function is also a function of these two variables,

$$L(\mathbf{H}_{DC}(k_L, \Delta k_L)|\mathbf{x}) = \prod_{i=1}^{n} P(d_i|\mathbf{H}_{DC}(k_L, \Delta k_L)) \tag{7}$$

As a heavy-tailed distributions for $P(x)$, we used a Lorentzian,

$$P(k_L, \Delta k_L, k_0) = N \frac{\Delta k_L}{\Delta k_L^2 + (k_L - k_0)^2} \tag{8}$$

where the normalisation factor N is chosen so that the integral of P from $k_L = -1$ to 1 is unity. Then the likelihood for $\mathbf{H}_{DC}$ is

$$L_{DC}(\Delta k_L, k_0) = \prod_{i=1}^{n} P_{DC}(\Delta k_L, k_0) \tag{9}$$

L_{DC} is plotted in Fig.5 as a function of k_L and Δk_L, and we see that the maximum likelihood $L_{DC} \sim 3$ occurs at $k_L = 0.2$, or $k = 1.6$, in reasonable agreement with the $k = 0.68$ given by the direct fit to the Fig.2a datasets or the $k = 1$ used in Fig.1a. The maximum $L_{DC} \sim 3$ means that the odds on $\mathbf{H}_{DC}$ and against $\mathbf{H}_{HP}$ are three to one. This is already a strong indication that $\mathbf{H}_{DC}$ will be the preferred hypothesis.

To include the significance of the number of parameters p, we now calculate the value AIC of the AIC, given by

$$AIC = 2p - 2\ln L \tag{10}$$

where p is the number of parameters, so we have

$$AIC_{HP} = 68 - 2\ln L_{HP} = 68$$
$$AIC_{DC} = 36 - 2\ln L_{DC} = 33.8 \tag{11}$$

The relative likelihood of the hypothesis with the lower AIC, here $\mathbf{H}_{DC}$, is

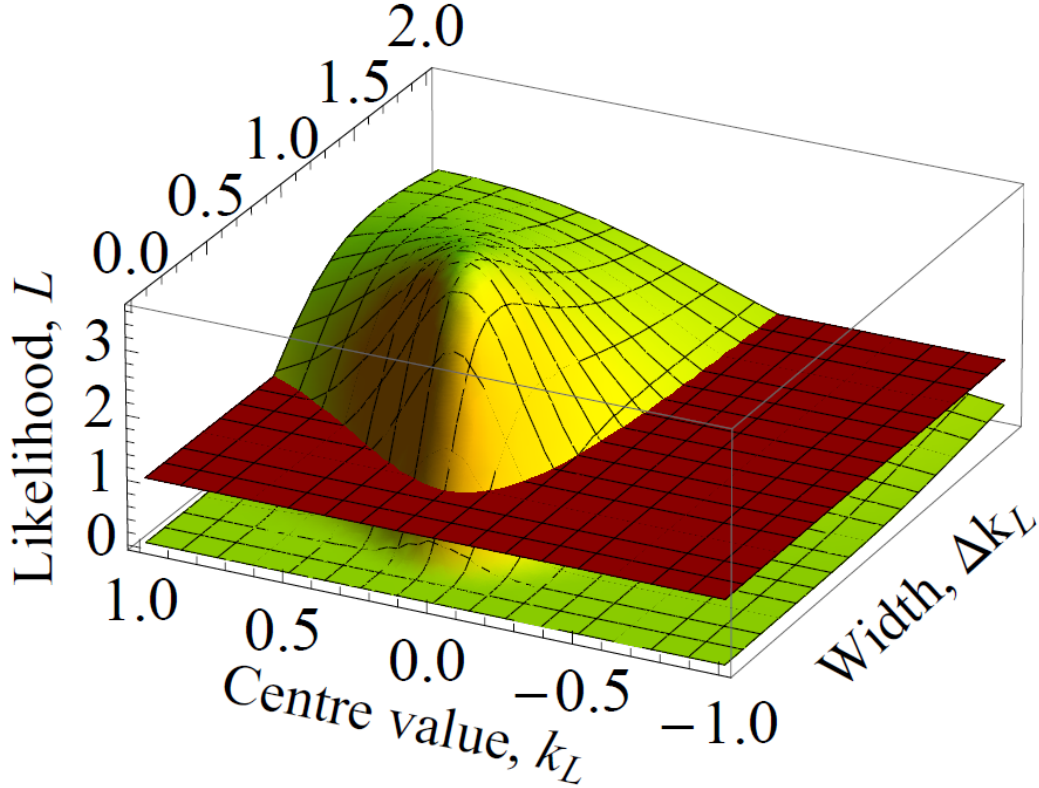$$AIC = e^{-\frac{1}{2}(AIC_{HP} - AIC_{DC})} = 3.7 \times 10^8 \tag{12}$$

Fig.5. The likelihood functions L_{HP} (the flat plane at $L = 1$) and L_{DC} given by Eq.9 are plotted against k_L and Δk_L. The peak height value for $\mathbf{H}_{DC}$ is $L = 3$, occurring at the value $k_L = 0.2$ and width $\Delta k_L = 0.6$, consistent with $k \sim 1$.

The hypothesis $\mathbf{H}_{DC}$ is overwhelmingly favoured by odds of many millions to one. This analysis quantifies the informal reasoning (by Occam's Razor) that it would be highly unlikely, if the Hall-Petch Eq.2 were a true reflection of reality with two independent parameters per dataset, that a substantial subset of the data would fit Eq.4 (Fig.2a). It confirms and expresses quantitatively the informal reasoning that if there exist plausible *ad-hoc* explanations of the data of Fig.2c which disagree with $\mathbf{H}_{DC}$, then these data are not strong evidence against $\mathbf{H}_{DC}$ nor strong evidence for the counter hypothesis $\mathbf{H}_{HP}$.

It is worth noting that the values *AIC* and *BIC* returned by the *Mathematica*[©] function *NonlinearModelFit* in fitting all 17 datasets simultaneously to Eq.2 with 34 free parameters and to Eq.4 with 18 parameters do prefer strongly the Hall-Petch fit. This is an artefact arising from the assumption in the *Mathematica*[©] analysis that the residuals on the fits are Gaussian-distributed. This assumption penalizes models with heavy-tailed distributions very severely.

3. Theory and Discussion

3.1. *Theories of the inverse-square-root dependence.*

There are several theoretical explanations extant in the literature to explain the inverse square-root of grain size appearing in Eq.2. See Conrad and Jung (2005) or Zhu *et al*. (2008) for a discussion.

Hall (1951) used the inverse square-root fit (Eq.2) because of the theory of Eshelby *et al*. (1951) of dislocation pile-up. Subsequently, as more experimental data became available and appeared to support the inverse square-root fit, this developed into the idea that a stress concentration factor should be invoked to account for plasticity. In a macroscopic picture, slip bands originate in a single grain, and propagate across grain boundaries under a sufficient stress. In a microscopic picture, dislocations emitted by the same source pile up against the grain boundary until the stress concentration is sufficient to cause emission of dislocations in the next grain. In two-dimensional DDD, Balint *et al*. (2005) used impermeable grain boundaries and found pile-up and strengthening according to Eq.2. This is not surprising, since dislocations are confined to the same slip planes and cannot bow out as bowing requires three dimensions. However, pile-up is not always observed in experiment (e.g. Li and Chou, 1970) nor in three-dimensional DDD. Simulations of bicrystals under uniaxial loading (Daveau, 2012) have shown that grain boundaries do not, of themselves, cause pile-up. Zhou and LeSar (2012), using both impenetrable and penetrable grain boundaries, observe that many dislocations embed into the simulated grain boundaries instead of piling-up, and that the others form a more complex structure. Senger *et al*. (2013) do observe pile-up under suitable conditions but that it has little influence on the stress. Admittedly, DDD simulation are restricted to low values of strain $\varepsilon \sim 0.02$, but this is ample to observe the Hall-Petch effect on the yield and flow strains and to observe pile-up under suitable conditions. In these simulations, the grain boundaries are usually modelled as simple impenetrable surfaces, e.g. Balint *et al*. (2005), LeSar (2012) – it is hard to envisage a more sophisticated model that would be still more conducive to pile-up.

Since pile-up is not always observed or not always important, other theories have been proposed. There are three physically-distinct models in which the inverse square-root derives from the Taylor expression for the shear flow stress τ in forest hardening, $\tau = \tau_0 + \alpha\mu b\rho^{1/2}$ where α is a factor of the order of unity, μ is the shear modulus, *b* is the magnitude of relevant components of the Burgers vector and ρ is the dislocation density. Then a direct dependence of the dislocation density ρ on the inverse of the length scale, here d^{-1}, is invoked. Ashby (1970) proposed that the variations in properties from grain to grain necessitate inhomogeneous plastic strain, and hence densities ρ of geometrically-necessary dislocations which will contribute to hardening. The magnitudes of the resulting plastic strain gradients scale with d^{-1} giving $\rho \propto d^{-1}$. The inverse square-root in the Hall-Petch law then derives directly from the square root in the Taylor formula. Li (1963) proposed that grain boundaries act as dislocation sources, and again the inverse square-root in the Hall-Petch law derives directly from the Taylor formula. Finally the Conrad slip-distance theory (Conrad and Jung, 2005) has a dislocation density proportional to the inverse of the slip distance or mean free path of mobile dislocations,

which here is dependent on the grain size. In the Conrad theory, the Hall-Petch inverse square-root again derives from the Taylor formula; also it occurs only with square-root strain-hardening as $\tau(\varepsilon_{pl}) - \tau_0 \propto \varepsilon_{pl}^{\frac{1}{2}}$.

It is not clear to what extent these theories require that the scaling exponent is rigorously $x = \frac{1}{2}$, and the data certainly provides no strong support for that value. The Eq.1 fitting parameters σ_0 and k, which are interpreted in terms of independent material properties, vary very much for any given data set according to the value of x used to fit the data, as seen in Fig.1. Yet these theories do not predict that the two fitting parameters σ_0 and k should vary together from one material to another in the way required by Fig.2a, such that so many datasets should fit accurately Eq.3 with only one free fitting parameter (σ_0) for each dataset.

3.2. *Dislocation Curvature*

A valuable insight comes for DDD simulations, which have no intrinsic length scale. On assigning a length scale ℓ to any given simulation, dislocation curvatures change as the inverse of that length scale and so do the corresponding stresses. The evolution of the simulation is, of course, independent of the length scale assigned.   This is sufficient to show that over-stresses – whether yield or flow stresses – and the corresponding elastic yield or flow strains, should scale with ℓ^{-1}. This is the physical basis for Eq.3 above (Dunstan *et al.* 1996, Dunstan 2012). Then details of the dislocation self-energy modify this to give the $\ell^{-1} \ln \ell$ form of Eq.4. This scaling behaviour is seen in Matthew's (1966) equilibrium critical thickness theory for the plastic relaxation of strained epitaxial layers, in which the radius of curvature of the termination of a misfit dislocation, equal to the layer thickness h, determines how the stress required for plasticity must vary with the thickness (as $h^{-1} \ln h$).

A more mechanistic account of the physical origin of the scaling laws Eq.3 and Eq.4 takes into account directly the line tension or energy per unit length of a dislocation. The displacement of material due the introduction of a dislocation is, of course, the constant b. This means that the stress required scales inversely with the dimension L of the material displaced through b. This is the physical origin of the L^{-1} term in Eq.3 and Eq.4. An excellent example, studied intensively both experimentally and theoretically, is found in the analysis of strained epitaxial layers. Following Matthews (1966), plastic relaxation requires a layer thickness large enough to put sufficient force on a threading dislocation to turn it over and extend it as a misfit dislocation (Matthews critical thickness).

The dislocation energy consists of a contribution from the core (atomistic) and a contribution from the elastic energy of the strain field of the dislocation. This elastic energy is found by integration over the radius from the dislocation, and to avoid divergence the integral has to be cut off an inner radius $r_0 \sim b$ and at an outer radius R_0 which is given by a free surface, or by the distance to other dislocation or other parts of the same dislocation (e.g. in the case of a dislocation dipole). This is the physical origin of the logarithmic term in Eq.4 (Cottrell 1953). It should be included in analysis of any problem invoking dislocation bowing such as precipitation hardening (Monnet, 2006) or forest hardening (Madec *et al.*, 2002). Madec *et al.* show in a DDD study of forest

hardening that over six orders of magnitude of dislocation density the influence of the logarithmic term is clearly detectable.

Significant plasticity requires that dislocation sources operate. In the application to strained epitaxial layers, this requires a thickness a few times Matthews critical thickness, so that relaxation critical thickness can be defined as a few times equilibrium critical thickness (Beanland, 1995; Dunstan *et al.*, 1996; Dunstan, 2012). It also eliminates the need to include an unstrained substrate in the problem, and therefore applies to micromechanical testing in general. More generally, the Matthews approach applies to dislocation source operation in any confining volume. Parthasawary *et al*. (2007) and Huang *et al*. (2011) have used the same idea to account for the size effect in micropillars where it is the diameter of the pillar that constrains the source, as also have Gruber *et al*. (2008) for the strengthening of thin films. Most generally, it applies to the overstress called the size effect in nanoindentation and micromechanics, whenever spatial confinement over a length scale ℓ puts a lower bound on dislocation curvature and hence on stress, as we have proposed previously (Jayaweera, 2003; Dunstan and Bushby, 2004). And here we suggest that Fig.2a and the statistical analysis in Section 2 of the models $\mathbf{H}_{HP}$ and $\mathbf{H}_{DC}$ is strong evidence that it applies to the effect of grain size on the strength of metals as well. That is, a size effect is seen whenever dislocation curvature is restricted by the space in which it has to operate.

This approach predicts a minimum strength of k/L where L is the relevant length scale restricting the dislocation bowing radius. L need not be grain size; L may be structure size, dislocation spacing, precipitate spacing, etc, or some suitable combination of these factors. The relationship to the models of Section 3.1 is thus that if these models invoke bowing or source operation, they must predict at least the minimum strength. As in the superposition of precipitation hardening and forest hardening studied by Queyreau *et al.* (2010), each extra strengthening mechanism may also have a length scale and a scaling exponent. This may be treated by constructing a combined effective length. Or, as we do in this paper, the effective length is identified with the grain size, and to the extent that the other models give an extra contribution to the strength, then this may contribute to what we have called the bulk strength. In that case it could also give rise to the deviations above our fits observed on the right-hand side of Fig.2c. Different such mechanisms could very well occur at different length scales resulting in the identification of distinct size regimes, as proposed by Kraft 2010. Nevertheless, our analysis in this paper leads to the conclusion that the data provides evidence for only one exponent, which is unity.

4. Conclusions

Here, we have demonstrated two rather separate conclusions:
The first is that there is no conclusive experimental evidence for the inverse square-root dependence of strength upon grain size, the Hall-Petch law, despite the rare datasets such as Ti (Hu and Cline, 1968) which fit this particularly well. The uncertainty in the exponent is great enough that the simple inverse fits or inverse fourth-root fits may be as good. This implies that the exponent should also be a fitting parameter (Eq.1) rather than fitting to the two parameters of Eq.2. In this case, the strong correlations in the fitted

15

parameter values should be taken into account when a physical interpretation of their values is sought;

The second conclusion is that the k values observed as the exponent x is varied collapse onto a single k value for the simple inverse ($x = 1$). This is a very strong indication that the different materials, and indeed differently treated specimens of the same material, are distinguished by a single parameter value σ_0 for each specimen that expresses its different asymptotic limit (yield or flow strength at infinite grain size), and that after suitable normalization of the data the size effect is described by a second parameter k with the same value for all materials, as in Eq.3 or Eq.4. Moreover, there is a sound physical basis for supposing the validity of this approach.

Following these two conclusions, the Hall-Petch dependence of the strength on grain size is another manifestation of the same size effect as observed in epitaxial layers and in micromechanical testing.

Acknowledgements

References

Akaike, H., 1974. A new look at the statistical model identification. System identification and time-series analysis. IEEE Trans. AC-19, 716-723.

Armstrong, R., Codd, I., Douthwaite, R.M., Petch, N.J., 1962. The plastic deformation of polycrystalline aggregates. Phil. Mag. 7, 45–58.

Armstrong, R.W., 2011. Strength and strain-rate sensitivity of nanopolycrystals, in *Mechanical properties of nanocrystalline materials*, ed. James C.M.U. (Pan Stanford Publishing) ch.3.

Armstrong, R.W., Jindal, P.C., 1968. On the hardness and recrystallized grain size of alpha titanium. Trans. TMS-AIME. 242, 2513.

Armstrong, R.W., Elban, W.L., 2012. Hardness properties across multi-scales of applied loads and material structures. Mater. Sci. & Technol. 28, 1060 –1071.

Arzt, E., 1998. Size effects in materials due to microstructural and dimensional constraints: A comparative review. Acta Mater. 16, 5611–5626.

Ashby, M.F., 1970. The deformation of plastically non-homogeneous materials. Phil. Mag. 21, 399–424.

Babyak, W.J., Rhines, F.N., 1960. The relationship between the boundary area and hardness of recrystallized cartridge brass. Trans. TMS-AIME, 218, 21–23.

Balint, D.S., Deshpande, V.S., Needleman, A., Van der Giessen, E., 2005. A discrete dislocation plasticity analysis of grain-size strengthening. Mat. Sci. Eng. A 400–401, 186–190.

Bassett, W.H., Davis, C.H., 1919. Comparison of grain-size measurements and Brinell hardness of cartridge brass. Trans. TMS-AIME. 60, 428–449.

Beanland, R., 1995. Dislocation multiplication mechanisms in low-misfit strained epitaxial layers. J. Appl. Phys. 77, 6217–6222.

Benford, F., 1938. The law of anomalous numbers. Proc. Am. Philo. Soc. 78, 551–572.

Brittain, C.P., Armstrong, R.W., Smith, G.C., 1985. Hall-Petch dependence for ultrafine grain size electrodeposited chromium. Scripta Metall. 19, 89–91.

Bushby, A.J., Dunstan, D.J., 2004, Plasticity size effects in nanoindentation, J. Mater. Res. **19**, 137–142.

Bushby, A.J., Dunstan, D.J., 2011. Size effects in yield and plasticity under uniaxial and non-uniform loading: experiment and theory. Phil. Mag. 91, 1037–1049.

Conrad, H., Jung, K., 2005. Effect of grain size from millimetres to nanometers on the flow stress and deformation kinetics of Ag. Mater. Sci. Eng. A391, 272–284.

Cottrell, A.H., 1953. *Dislocations and Plastic Flow in Crystals* (Clarendon Press, Oxford).

Daveau, G., 2012. "Interaction dislocations – joints de grains en deformation plastique monotone : étude expérimentale et modélisations numériques." Thesis, Ecole Centrale, Paris, http://zig.onera.fr/~devincre/perso_html/Documents/PhD_Daveau.pdf

Dunstan, D.J., 2012. Critical thickness theory applied to micromechanical testing. Adv. Eng. Mater. 14, 942–947.

Dunstan, D.J., Kidd, P., Beanland, R., Sacedón, A., Calleja, E., González, L., González, Y., Pacheco, F.J., 1996. Predicability of plastic relaxation in metamorphic epitaxy. Materials Science and Technology 12, 181–186.

Dunstan, D.J., Ehrler, B., Bossis, R., Joly, S., P'ng, K.M.Y., Bushby, A.J., 2009. Elastic limit and strain hardening of thin wires in torsion. Phys. Rev. Lett. 103, 155501.

Dunstan, D.J., Bushby, A.J., 2013. The scaling exponent in the size effect of small scale plastic deformation. Int. J. Plasticity 40, 152–162.

Embury, J.D., Fisher, R.M., 1966. The structure and properties of drawn pearlite. Acta Metall. 14, 147–159.

Ehrler, B., Hou, X.D., Zhu, T.T., P'ng, K.M.Y., Walker, C.J., Bushby A.J., Dunstan, D.J., 2008. Grain size and sample size interact to determine strength in a soft metal. Phil. Mag. 88, 3043–3050.

Eshelby, J.D., Frank, F.C., Nabarro, F.R.N., 1951. The equilibrium of linear arrays of dislocations. Phil Mag. 42, 351–364.

Gruber, P.A., Böhm, J., Onuseit, F., Wanner, A., Spolenak, R., Arzt, E., 2008. Size effects on yield strength and strain hardening for ultra-thin Cu films with and without passivation: A study by synchrotron and bulge test techniques. Acta Mat. 56, 2318-2355.

Hall, E.O., 1951. The deformation and ageing of mild steel: III Discussion of results. Proc. Phys. Soc. B64, 747–753.

Hodge, A.M., Biener, J., Hayes, J.R., Bythrow, P.M., Volkert, C.A., Hamza, A.V., 2007. Scaling equation for yield strength of nanoporous open-cell foams. Acta Mat. 55, 1343–1349.

Hu, H., Cline, R.S., 1968. Mechanism of reorientation during recrystallization of polycrystalline titanium. Trans. TMS-AIME. 242, 1013–1024.

Huang, L., Li, Q.-J., Shan, Z.-W., Li, J., Sun, J., Ma, E., 2011. A new regime for mechanical annealing and strong sample-size strengthening in body centred cubic molybdenum. Nature Comm. 2, 547.

Jang, J.S.C., Koch, C.C., 1990. The Hall-Petch relationship in nanocrystalline iron produced by ball milling. Scripta Met. Mater. 24, 1599–1604.

Jayaweera, N.B., Downes, J.R., Frogley, M.D., Hopkinson, M., Bushby, A.J., Kidd, P., Kelly A., Dunstan, D.J., 2003. The onset of plasticity in nanoscale contact loading, Proc. Roy. Soc. London, A459, 2049–2068.

Jindal, P.C. and Armstrong, R.W., 1967. The dependence of the hardness of cartridge brass on grain size. Trans. TMS-AIME. 239, 1856–1857.

Korte, S. and Clegg, W.J., 2011. Discussion of the dependence of the size effect on the yield stress in hard materials studied by microcompression of MgO. Philosophical Magazine 91, 1150–1162.

Kraft, O., Gruber, P.A., Mönig., R., Weygand, D., 2010. Plasticity in confined dimensions. Ann. Rev. Mater. Res. 40, 293–317.

Li, J.C.M., 1963. Petch relation and grain boundary sources. Trans. TMS-AIME 227, 239–247.

Li, J.C.M., Chou, Y.T., 1970. The role of dislocations in the flow stress – grain size relationships. Met. Trans. 1, 1145–1159.

Liu, D., He, Y., Dunstan, D.J., Zhang, B., Gan, Z., Hu, P., Ding, H., 2013. Towards a further understanding of size effects in the torsion of thin metal wires: An experimental and theoretical assessment, Int. J. Plasticity 41, 30–52.

Liddle, A.R., 2007. Information criteria for astrophysical model selection. Monthly Notices of the Royal Astronomical Society: Letters, 377: L74–L78.

McKay, D.J.C., 2003. *Information theory, inference and learning algorithms* (Cambridge University Press, Cambridge) ch.3.

Madec, R., Devincre, B., Kubin, L.P., 2002. From dislocation junctions to forest hardening. Phys. Rev. Lett. 89, 255508.

Matthews, J.W., 1966. Accomodation of misfit across the interface between single-crystal films of various face-centred cubic metals. Phil. Mag. 13, 1207–1221.

Monnet, G., 2006. Investigation of precipitation hardening by dislocation dynamics simulations. Phil. Mag. 86, 5927–5941.

Orowan, E., 1947. Symposium on Internal Stresses. Institute of Metals, London, p. 45.

Newcomb, S., 1881. Note on the frequency of use of the different digits in natural numbers. Am. J. Math. 4, 39–40.

Parthasarathy, T.A., Rao, S.I., Dimiduk, D.M., Uchic, M.D., Trinkle, D.R., 2007. Contribution to size effect of yield strength from the stochastics of dislocation source lengths in finite samples. Scripta Mat. 56, 313–316.

Petch, N.J., 1953. The cleavage strength of polycrystals. J. Iron Steel Inst. 174, 25–28.

Queyreau, S., Monnet, G., Devincre, B., 2010. Orowan strengthening and forest hardening superposition examined by dislocation dynamics simulations. Acta Mat. 58, 5586–5595.

Senger, J., Weygand, D., Dunstan, D.J., 2013. *Presented at Plasticity 2013*

Vashi, U.K., Armstrong, R.W. and Zima, G.E., 1970. The hardness and grain size of consolidated fine tungsten powder. Metall. Trans. 1, 1769–1771.

Zhou, C., LeSar, R., 2012. Dislocation dynamics simulations of plasticity in polycrystalline thin films. Int. J. Plasticity 30-31, 185–201.

Zhu, T.T., Bushby, A.J. and Dunstan, D.J., 2008. Materials mechanical size effects: A review. Materials Technology **23**, 193–209.

Table I. Normalisation and Fitting Parameters

Metal	Normalisation parameters		Hall-Petch fit parameters, normalised Eq.2, $x = \frac{1}{2}$		Fit parameters, normalised Eq.1			Fit parameters, normalised Eq.4, $x = 1$	
	Y GPa	a_0 nm	ε_0	k	ε_0	k	x	ε_0	k
Nano-Fe [a]	211	0.287	2.57×10^{-3}	0.054	3.2×10^{-3}	0.070	0.60 ± 0.2	3.90×10^{-3}	0.075 ± 0.01
Nano-Fe [b]	211	0.287	3.08×10^{-4}	0.14	2.4×10^{-3}	0.54	0.78 ± 0.08	2.08×10^{-3}	0.36 ± 0.01
Ti [c]	116	0.295	3.0×10^{-3}	0.10	2.9×10^{-3}	1.02	0.50 ± 0.04	3.55×10^{-3}	0.37 ± 0.02
W [d]	411	0.316	2.5×10^{-3}	0.185	4.3×10^{-3}	3.4	0.99 ± 0.25	4.06×10^{-3}	0.58 ± 0.04
Cr [e]	279	0.288	1.76×10^{-3}	0.20	2.1×10^{-3}	0.37	0.60 ± 0.05	2.88×10^{-3}	0.72 ± 0.03
Cu [f]	115	0.361	2.10×10^{-4}	0.055	3.4×10^{-4}	0.0028	0.20 ± 0.5	2.7×10^{-4}	0.90 ± 0.02
Fe Fig3.1	211	0.287	5.5×10^{-4}	0.14	1.45×10^{-4}	0.041	0.34 ± 0.05	9.1×10^{-4}	0.91 ± 0.01
CuZn YP [f]	115	0.361	4.1×10^{-4}	0.136	1.75×10^{-4}	0.046	0.37 ± 0.08	7.1×10^{-4}	1.25 ± 0.1
Steel 2.5% [g]	211	0.287	8.9×10^{-4}	0.092	1.14×10^{-3}	0.0085	0.84 ± 0.15	9.9×10^{-4}	1.36 ± 0.25
CuZn 20% [f]	115	0.361	2.95×10^{-4}	0.154	3.0×10^{-3}	0.154	0.38 ± 0.14	3.3×10^{-3}	1.43 ± 0.02
Steel [h]	211	0.287	3.0×10^{-4}	0.156	4.6×10^{-4}	0.63	0.65 ± 0.2	5.9×10^{-4}	1.8 ± 0.2
Steel 20% [g]	211	0.287	1.62×10^{-3}	0.131	2.0×10^{-4}	0.0089	1.00 ± 0.2	1.77×10^{-3}	2.2 ± 0.2
Steel YP [g]	211	0.287	3.7×10^{-4}	0.22	1.54×10^{-4}	0.31	0.51 ± 0.03	5.7×10^{-4}	3.8 ± 0.3
CuZn6931 [i]	115	0.287	1.03×10^{-3}	0.31	1.00×10^{-3}	0.41	0.52 ± 0.1	1.3×10^{-3}	5.5 ± 0.3
CuZn7030 [j]	115	0.361	8.6×10^{-4}	0.28	6.6×10^{-4}	0.46	0.52 ± 0.1	1.1×10^{-3}	5.5 ± 0.4
CuZn6832 [i]	115	0.361	9.0×10^{-4}	0.36	1.27×10^{-3}	6.5	0.75 ± 0.14	1.3×10^{-3}	6.5 ± 0.04
Fe [k]	211	0.287	2.1×10^{-3}	0.52	2.5×10^{-3}	3.1	0.68 ± 0.2	2.8×10^{-3}	7.4 ± 0.25

[a] Nanocrystalline iron, Jang and Koch (1990), taken from Armstrong (2011) Fig.1.

[b] Nanocrystalline iron, Embury and Fisher (1966), taken from Armstrong (2011) Fig.1.

[c] Recrystallised titanium, Hu and Cline (1968), taken from Armstrong and Jindal (1968) Fig.1

[d] Powder-compacted tungsten, Vashi *et al.* (1970), taken from Armstrong and Elban (2012) Fig.21

[e] Electro-deposited chromium, Brittain *et al.* (1985) Fig.1.

[f] Copper at 0.5% strain, brass at yield point and at 20% strain, Armstrong *et al.* (1962) Fig.3

[g] Steel at yield point, 2.5% and 20% strain, Armstrong *et al.* (1962) Fig.1

[h] Annealed mild steel – Armco, Siemens-Martin, basic Bessemer – Hall (1951) Fig.1a

[i] 68-32 and 69-31 brass, Bassett and Davis (1919) taken from Jindal and Armstrong (1967) Fig.1.

[j] Rolled and annealed cartridge brass, Babyak and Rhines (1960) taken from Jindal and Armstrong (1967) Fig.1.

[k] Mild steel, ingot iron, spectrographic iron, Petch (1953) Fig.1.